The Effects of Aggregation on Electronic and Optical Properties of Oligothiophene Particles

David P. Ostrowski, Lauren A. Lytwak, Michelle L. Mejia, Keith J. Stevenson, Bradley J. Holliday, and David A. Vanden Bout*

Department of Chemistry and Biochemistry, The University of Texas at Austin, 1 University Station A5300, Austin, Texas 78712-0165, United States

ABSTRACT

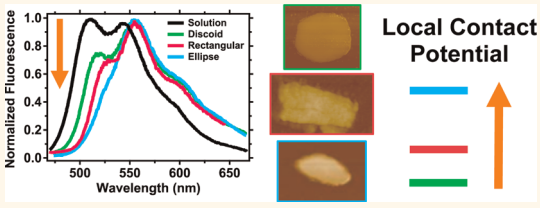

Solution processing of oligothiophene molecules is shown to produce a range of particles with distinct morphologies. Once isolated on a substrate, the optical and electronic properties of individual particles were studied. From polarized scanning confocal microscopy experiments, distinct particles that are identifiable by shape were shown to have similar emission spectra except in regard to the 0—0 vibronic band intensity. This suppression of the 0—0 vibronic band correlates to the amount of energetic disorder present in a weakly coupled H-aggregate. The studied particles ranged from moderate to almost complete suppression of the 0—0 vibronic band when compared to the emission spectrum of the isolated molecule in solution. All particles were found to have a high degree of geometric order (molecular alignment) as observed from the fluorescence dichroism (FD) values of around 0.7—0.8 for all the studied morphologies. The structural and electronic properties of the particles were investigated with Kelvin probe force microscopy (KPFM) to measure the local contact potential (LCP) difference, a quantity that is closely related to the differences in intermolecular charge distribution between the oligothiophene particles. The LCP was found to vary by as much as 70 mV between different oligothiophene particles and a trend was observed that correlated the LCP changes with the amount of energetic disorder present, as signified by the suppression of the 0—0 vibronic peak in the emission spectra. Combined polarized scanning confocal microscopy studies, along with KPFM measurements, help to provide fundamental insights into the role of morphology, molecular packing, and intermolecular charge distributions in oligiothiophene particles.

KEYWORDS: oligothiophene · morphology · aggregate · spectroscopy · Kelvin probe force microscopy

New environmentally friendly energy sources are needed to meet the world's increasing demand for energy.[1] Solution processable photovoltaic materials show promise due to their low cost and scalability. However, the efficiency of these technologies remains well below the threshold required for commercial viability.[2] One factor affecting the photovoltaic properties of these materials is molecular morphology, in particular, the extent to which a molecule is electronically coupled (aggregated) to neighboring molecules.[3−5] Within a solution-deposited thin film, the local morphology has been observed to vary substantially across the film, ranging from amorphous to highly aggregated.[6−11] Thus, design and control of optimized materials for efficient charge separation requires a fundamental understanding of the role that these morphological variations have on the optical and electronic properties of a material.

This work presents a study of how morphology, specifically molecular aggregation, affects optical and electronic properties. Different solution processing conditions were used to produce a variety of particle morphologies from the same conjugated small molecule. While this method produced numerous random and undistinguishable particles, there were also a number of consistently occurring particle shapes formed that were microscopically identifiable. These identifiable particles were found to have similar optical and electronic properties as other particles of the same shape. However, distinct optical and electronic properties were observed for each different shape of particle studied. Typically, differences in molecular aggregation result in variations of the optical properties of the aggregates.[12,13] Herein, we show that molecular aggregation also affects the electronic properties of the molecules, in particular the local contact potential (LCP) difference of the material as deduced from Kelvin probe force microscopy (KPFM) measurements. This variation of the electronic properties with morphology has clear implications for understanding the relative energy level changes of organic materials in solution-processed films used for bulk heterojunction photovoltaics.

* Address correspondence to davandenbout@mail.utexas.edu.

Received for review March 30, 2012 and accepted May 16, 2012.

Published online May 16, 2012
10.1021/nn301410j

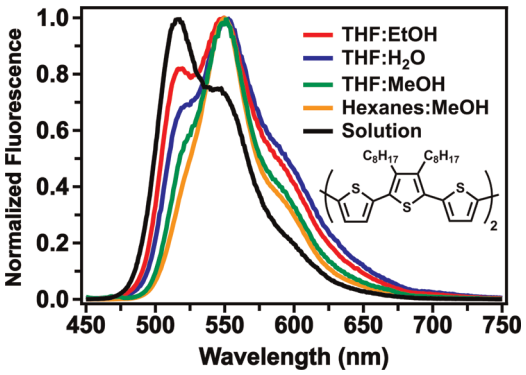

Figure 1. Emission spectra from the O6T particles that resulted from solution processing with different solvent combinations, along with the spectrum of O6T in THF solution. The solution spectrum was shifted 8.5 nm higher in wavelength to allow better comparison with the other spectra. The particles were drop cast onto a glass substrate for analysis. Inset shows structure of O6T molecule.

RESULTS AND DISCUSSION

The structure of the oligothiophene molecule, 3′,3‴′,4′,4‴′-tetraoctyl-2,2′:5′,2″:5″,2‴:5‴,2⁗:5⁗,2⁗′:5⁗′,2⁗′′-sexithiophene (O6T), used in this work is shown in the inset of Figure 1. Particles of O6T were fabricated by injecting 100 μL of an O6T solution into 10 mL of a stirred "bad" solvent (one O6T is only partially or not soluble in but that is miscible with the solvent used for the initial solution of O6T). As the O6T molecules are forced out of solution, O6T particles are formed. The resulting colloidal suspension of O6T particles can then be drop cast onto a substrate. Drop casting isolates the particles, allowing for optical and electronic studies of individual aggregates. Once isolated, the particles were studied with a variety of characterization techniques including: fluorescence spectroscopy, polarized scanning confocal microscopy, scanning electron microscopy (SEM), atomic force microscopy (AFM) and Kelvin probe force microscopy (KPFM).

The ensemble average emission spectrum (collected from a substrate containing a set of deposited particles from a particular solvent combination) were studied with a standard fluorometer. Figure 1 shows these ensemble emission spectra from the particle sets prepared from different solvent combinations, along with the spectra from solvated O6T molecules in a tetrahydrofuran (THF) solution. The solvated emission spectrum of O6T shows a typical vibronic progression dominated by a single vibrational mode. The emission spectra of the particle sets are similar, except with regard to the intensity of the highest energy 0−0 vibronic band, which varies in intensity as the solvent combination is changed. Theoretical work from Spano *et al.* has shown that the suppression of the 0−0 vibronic band in the emission spectrum to be a characteristic of weakly coupled H-aggregates, with the intensity of the 0−0 band in the emission spectrum being related to the extent of energetic disorder present in the aggregate.[13,14] Figure 1 demonstrates that the 0−0 band intensity varies between particles prepared from different solvent combinations, indicating that the nature of these aggregates could be tuned through solution processing.

For investigating the geometric heterogeneity and physical shape of the particles, AFM and SEM were used. For any given particle sample set from a particular solvent combination, a number of identifiable morphologies were observed along with other aggregates of less defined morphology. As the identifiable particles had a distinct and reproducible shape, it was possible to classify particular aggregates as belonging to one or another morphology and to correlate their optical and electronic properties as measured in two distinct experiments. The main morphologies targeted for this study were those formed from the THF/H_2O and THF/methanol (`good'/'bad') solvent combinations. These samples contained particles that clustered into a small number of distinct shapes.

To study the optical properties of individual particles, polarized scanning confocal microscopy was used (see Methods section). As a substrate containing isolated particles was raster scanned over the focused 408 nm excitation light, two-dimensional emission images were collected point-by-point in two orthogonal emission polarizations. After collecting these images, the excitation source could be repositioned onto a specific particle identified in the image to collect an emission spectrum of that individual particle. This allowed for correlation of particle shape and optical properties.

Figure 2a shows a fluorescence image collected from particles made from the THF/H_2O solvent combination. Two types of particles, identifiable by shape, were studied from this sample: the cylindrical particles called discoids and the oblong particles called ellipses. The two morphologies are identified in Figure 2a with green dots (discoid) and light blue dots (ellipse). Emission spectra were collected from a large number of discoid and ellipse particles to compare the two morphologies. Spectra collected from numerous particles of the same shape only showed slight spectral variations as shown in Figure 2b. Thus, different particles of the same shape possess similar morphological properties and molecular aggregation. Since nearly identical emission spectra are observed for similarly shaped particles, the spectra for numerous particles of each shape can be averaged together to better compare the two morphologies.

The averaged fluorescence spectra from both ellipse and discoid particles are shown in Figure 2c. The emission spectra for discoids and ellipses are similar except with regard to the intensity of the 0−0 vibronic band. There is the possibility that this is simply an effect of self-absorbance. However, the epi-illumination and collection geometry of the microscope allows for the

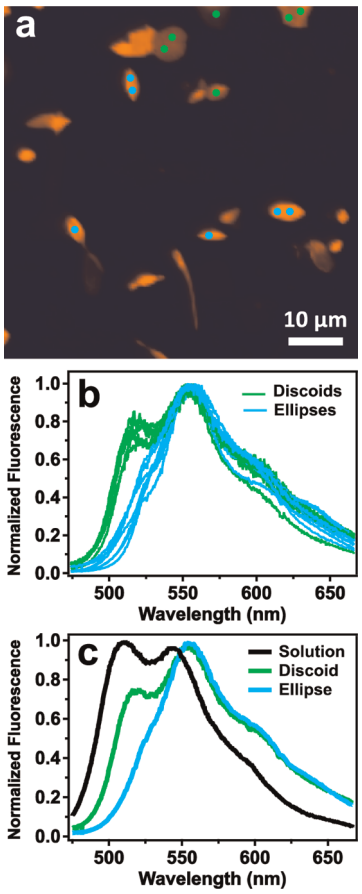

Figure 2. (a) Total fluorescence image obtained from scanning confocal microscopy of the THF/H_2O solvent combination particles drop cast onto a glass substrate. The intensity scale ranges from 100 to 37 500 counts. (b) Individual spectra of particles were collected at the blue points (ellipse) and green points (discoids) marked in image a. (c) Averaged spectra taken from numerous particles of elliptic (blue) or discoidal (green) morphology.

same absorption and emission depths from each particle measured; thus, any self-absorbance would be consistent for all particles. Additionally, some particles have essentially no 0−0 vibronic band emission intensity, which could not result solely form self-absorption given this geometry. There is also a lack of consistent correlation between particle brightness (which is an indication of particle thickness) and decreased intensity of the 0−0 vibronic band. As a result, this 0−0 vibronic band suppression is attributed to H-aggregate formation. For strongly coupled H-aggregates, one would expect no fluorescence as the emission is completely symmetry forbidden. However, for weakly coupled H-aggregates, only the 0−0 vibronic band is forbidden. This transition can be weakly allowed due to the breaking of symmetry in the aggregate by energetic disorder.[13,15] This disorder is characterized by two factors: the total energetic disorder (σ) and the spatial correlation of the disorder (β).[14,16] The intensity of the 0−0 emission peak is also affected by the free exciton bandwidth (W) and the Huang−Rhys factor (λ^2). From Figure 2c, it is observed that both the ellipse and the discoid spectra show some emission in the lowest energy 0−0 peak, but this emission is clearly suppressed when compared to the peak ratios of the O6T molecule isolated in a THF solution. To quantify the changes in the 0−0 vibronic band intensity, each emission spectrum was fit to a vibronic emission model consisting of a series of four Gaussian peaks separated by equal amounts of energy space (details and figures of the fits are included in the Supporting Information). The ratios of 0−0 to 0−1 band intensity were quantified from the Gaussian fits to the experimental data, and were 0.29, 0.64, and 0.93 for the ellipse, discoid, and solution spectra, respectively. The width of the peaks is reflective of the total energetic disorder (σ). Since the same peak width could be used to fit all the particle spectra, the value of the total energetic disorder (σ) is the same for all particles studied. Additionally, the Huang−Rhys factor (λ^2) is inherently the same for all the aggregates. The Huang−Rhys factor was determined to be 1.07 from the spectra of O6T molecules in solution. There are only two other parameters that can affect the intensity ratio of the 0−0 to 0−1 vibronic peaks: the values β and W.[14,16] To estimate possible variations in β, between the morphologies, an approximate value for W of 2000 cm^{-1} was used based on the results of previous studies.[15,17] The value of β, which can range between 0 and 1, was determined to be 0.37 and 0.65 for discoid and ellipse particles, respectively. From β, the spatial correlation length (ℓ_0) in dimensionless units of lattice spacing is determined through the relationship $\ell_0 = -1/\ln(\beta)$.[16] The spatial correlation length was found to range from 1.0 for discoid particles to 2.3 for ellipse particles. This shows that in the ellipse particles, the energetic disorder is correlated over a little more than twice as many molecules as in the discoid particles.

One possible source for the energetic disorder in the particles is geometric irregularities in the molecular packing. To compare the molecular order within each particle, polarized confocal images were collected to examine the emission polarization of each particle. The fluorescence collected during scanning confocal microscopy imaging of the sample was sent through a polarizing beam splitter, allowing for collection of the two orthogonal emission polarizations. The fluorescence images of the horizontal and vertical polarizations, defined in terms of the lab plane, are shown in Figure 3. From these images, the fluorescence dichroism (FD) can be determined at each pixel by calculating the difference between the two images divided by the sum. The FD is an indication of how well aligned the transition dipole moments are for a given sample. Since these particles are composed of the same molecule, the FD is an indication of the geometric order of the molecules within the particle. The FD values can range from −1 to 1; an FD value of 0 indicates there is

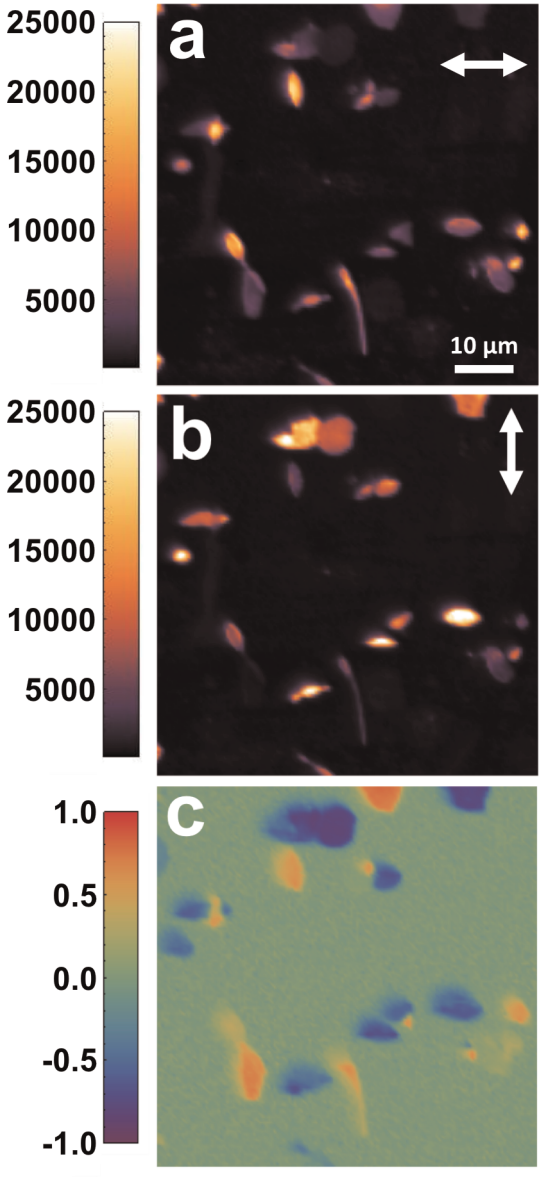

Figure 3. (a) Horizontally and (b) vertically polarized fluorescence images (defined in terms of the lab plane) obtained from polarized scanning confocal microscopy of the same particles shown in Figure 2. (c) Fluorescence dichroism (FD) image calculated from the fluorescence images a and b.

no distinct emission polarization and the sample is isotropic, which means there is no geometric alignment of the molecules. However, when FD is closer to −1 or 1, the sample has a distinct emission polarization and is well aligned. The FD values for the ellipse and discoid particles were 0.7 and 0.8, respectively. It is important to note that these are the minimum values possible, as no experimental methods were used to ensure that the emission polarization of a particle was completely aligned with one of the detectors. These high FD values indicate that the molecules within each particle are highly aligned and that the spectral differences must be a result of other factors such as intermolecular spacing.

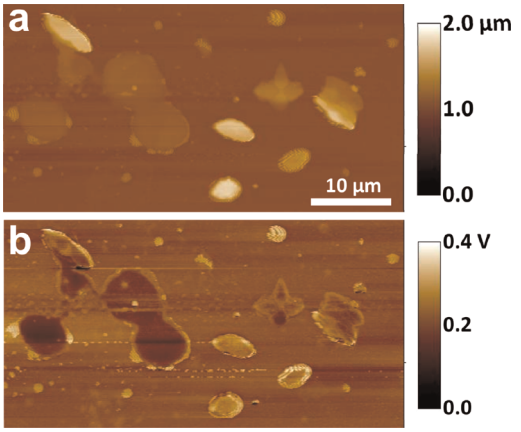

Figure 4. (a) Topography and (b) LCP images of ellipse and discoid particles on a glass substrate. Both images were linearly flattened for lucidity. Data analysis was performed on the unaltered images.

While the different particles have shown a distinguishable variation in optical properties, the question remains as to what affect, if any, these morphological differences have on electronic properties. For electronic property characterization, each particle was studied with KPFM. KPFM is a noncontact, nondestructive electronic technique that simultaneously measures structural features as well as the LCP difference between the scanning probe tip and the surface, which is closely related to intermolecular charge distribution.[18−27] First, the topographic AFM data are obtained and then the same line is rescanned at a specified lift height while the voltage difference between the AFM tip and the surface is determined at each point in the image. The bias voltage (V_{dc}) applied to the AFM tip is equal to the LCP difference between the tip and the surface, and is determined through nullification of the capacitance force between the tip and the surface. The LCP maps were measured for oligothiophene particles deposited on an insulating substrate (glass) to eliminate any electronic contributions from the underlying substrate. A representative topography and LCP image is shown in Figure 4. Data analysis was performed on unaltered images (example shown in Supporting Information) but for lucidity, both images in Figure 4 were linearly flattened. The LCP between ellipse and discoid particles was found to be 70 ± 30 mV. This LCP difference suggests that subtle morphological changes in particle shape and molecular packing are accompanied by a redistribution of charge within or between oligothiophene molecules. For instance, the local surface charge density (σ_{cd}) can be estimated by applying the Helmholtz equation for a parallel plate capacitor to the LCP measurement (more details in the Supporting Information).[28−32] For this calculation the permittivity of O6T was estimated to be 3 from the value for unsubstituted α-sexithiophene.[33] The higher surface potential for the ellipse particles corresponds to a higher σ_{cd} of ∼0.012 charges per nm^2 above the

discoid particles (assuming a capacitor thickness of 1 nm). Subtle changes in σ_{cd} (or intermolecular charge distribution) such as these could result from a variation in molecular packing density or molecular orientation between the different particles.

The variation in LCP suggests that the effective position of the highest occupied molecular orbital (HOMO) level of a molecule may shift at least 70 mV as a result of small changes in molecular packing and aggregation. As this difference was measured between particles of similar aggregation, the difference between amorphous and highly aggregated molecules could be even larger. This result correlates to a varying energy landscape in these π-conjugated material thin films as a result of the local morphology, which has been previously suggested.[34] Changes in the relative energy levels of a molecule with morphology would have an effect on the charge separation efficiency at a donor–acceptor interface and ultimately on the efficiency of thin film photovoltaic devices.

To investigate if this trend (decreased 0–0 vibronic band emission intensity correlating to an increased LCP) holds for more than just these two morphologies, a third particle from a different solvent combination was studied. Rectangular particles from the THF/methanol solvent combination were studied (see Supporting Information). The ratio of the 0–0 to 0–1 vibronic bands in the fluorescence spectrum of these particles was found to be 0.54, a slightly lower value than that of the discoid particles and in between the values for discoid and ellipse particles. The FD value again was high for these particles at 0.8, which shows that these particles also possess a high degree of molecular alignment. The LCP of the rectangular particles falls in between the values for the ellipse and discoid particles but is closer to the discoid value than the ellipse, which is expected based on the optical properties. The rectangular particle surface potential was $\sim 23 \pm 14$ mV higher than the discoid particles and $\sim 50 \pm 30$ mV lower than ellipse particles. These results show there is a correlated trend in the morphological effects on optical and electronic properties. More specifically, the suppression of the 0–0 vibronic band in the emission spectrum correlates to a decrease in the LCP of the particle, despite being composed of the same molecule.

CONCLUSIONS

This work demonstrates that morphology affects not only optical properties of a molecule but also electronic properties. Here, numerous identifiable particles were produced through solution processing of the same small molecule, O6T. Once the particles were isolated on a substrate, their individual properties could be studied and correlated. Emission spectra of particles of different shape showed a range of intensities in the 0–0 vibronic band as a result of variations in molecular aggregation between particles. Through KPFM, differences in the local contact potential and therefore changes in intermolecular charge distribution of distinct particles were measured. A direct correlation between optical and electronic properties of the different oligothiophene particle morphologies showed an observed trend; more well-defined aggregates (as signified by increased suppression of the 0–0 vibronic band intensity in emission spectra) also exhibit an increased LCP. This result signifies that these measurements are capable of detecting subtle variations in molecular packing density or molecular orientation between the different particle morphologies. From this result we can conclude that a thin film of organic materials composed of molecules with varying degrees of aggregation will have a correspondingly heterogeneous energy landscape. Given that the alignment of energy levels in a donor/acceptor system is known to affect charge separation, it is expected that the differences in local aggregation will have substantial effects on charge separation at bimolecular heterojunctions in thin film photovoltaics. Further studies are currently underway to correlate the effect molecular aggregation has in donor/acceptor systems through controlling aggregated states to optimize charge separation.

METHODS

Materials: Molecule and Particle Synthesis. The 3′,3‴″,4′,4‴″-tetraoctyl-2,2′:5′,2″:5″,2‴:5‴,2⁗:5⁗,2⁗′:5⁗′,2⁗′′-sexithiophene (O6T) particle fabrication included dissolving the molecule in a "good" solvent (one that O6T is soluble in) at 5 mM concentration and injecting 100 μL of that solution into 10 mL of a stirred "bad" solvent (one that O6T is only partially or not soluble in). The "good" solvents used include tetrahydrofuran (THF) and hexanes; the "bad" solvents used were nanopure water (H_2O), methanol (MeOH), and ethanol (EtOH). It is important that the solvent combination used be miscible. The particles from each solvent combination were isolated onto glass substrates through drop casting.

Fluorometer. The ensemble fluorescence spectra were collected with a SPEX Fluorolog 1 from Horiba Jobin Yvon that was controlled with LabVIEW. The excitation source was a 450 W xenon lamp, and two photomultiplier tube modules from Hamamatsu were used for detection of excitation and emission intensity.

Kelvin Probe Force Microscopy (KPFM). A Veeco Dimension 3100 atomic force microscope (AFM) with a Nanoscope IV controller was used to collect both the topographic and surface potential images. The cantilevers used were from MikroMasch (CSC21/Cr–Au) and had a ~105 kHz resonant frequency and 2.0 N/m spring constant. Images were collected under dark conditions in attractive mode with a lift height around 40 nm and drive amplitude around 2.5 V. For setting the drive phase, a standard sample step edge of chromium to gold metal was utilized. Typically, a drive phase of ~40° was used. As the absolute voltage of the instrument would drift over time, the particles surface potential was measured relative to the glass substrate

through a plot profile analysis as shown in Supporting Information, Figure S3c. Numerous measurements were collected from different particles of each shape and the reported surface potential differences were obtained by comparing the average of those values. The error in measurements were determined by error propogation of the noise in the instrument (~7.5 mV) with the standard deviation of the average potentials. The noise in the instrument was determined from the fluctuations in surface potential on a gold film.

Polarized Scanning Confocal Microscopy and Individual Particle Spectra. The confocal images were collected using a laboratory built microscope. The 408 nm excitation beam from a Coherent diode laser was focused onto the sample through a 60× Nikon objective with 0.7 numerical aperture. The fluorescence was collected through the same objective and isolated from the excitation with a dichroic mirror. A cube polarizing beam splitter was used to separate the fluorescence into two orthogonal polarizations that were imaged onto two Perkin-Elmer avalanche photodiodes (APDs). The polarizations were defined as I_x and I_y, with *X* and *Y* defined in terms of the lab plane. The sample was scanned through a two-dimensional piezo stage from Queensgate Instruments that was controlled by LabVIEW. After scanning, the LabVIEW program could be used to move the piezo stage to points of interest on the sample and the fluorescence rerouted from the APDs to an Acton spectrometer connected to a liquid-nitrogen-cooled charged coupled device (LN-CCD) from Princeton Instruments for collection of localized fluorescence spectra. The Gaussian fits to the spectra were performed with the Multipeak Fitting 2 analysis in Igor Pro.

Conflict of Interest: The authors declare no competing financial interest.

Acknowledgment. This work was supported as part of the program "Understanding Charge Separation and Transfer at Interfaces in Energy Materials (EFRC:CST)", an Energy Frontier Research Center funded by the U.S. Department of Energy, Office of Science, Office of Basic Energy Sciences under Award Number DE-SC0001091. The authors want to acknowledge K. Clark and C. Cone for help with collecting and analyzing the polarized scanning confocal microscope data.

Supporting Information Available: The data for the rectangular particles, the fitted emission spectra, details of the calculations for σ_{cd} and β, and a self-absorption analysis are presented. This material is available free of charge *via* the Internet at http://pubs.acs.org.

REFERENCES AND NOTES

1. Kamat, P. V. Meeting the Clean Energy Demand: Nanostructure Architectures for Solar Energy Conversion. *J. Phys. Chem. C* **2007**, *111*, 2834–2860.
2. Dennler, G.; Scharber, M. C.; Brabec, C. J. Polymer−Fullerene Bulk-Heterojunction Solar Cells. *Adv. Mater.* **2009**, *21*, 1323–1338.
3. Bredas, J. L.; Norton, J. E.; Cornil, J.; Coropceanu, V. Molecular Understanding of Organic Solar Cells: The Challenges. *Acc. Chem. Res.* **2009**, *42*, 1691–1699.
4. Yang, X.; Loos, J. Toward High-Performance Polymer Solar Cells: The Importance of Morphology Control. *Macromolecules* **2007**, *40*, 1353–1362.
5. Roncali, J.; Leriche, P.; Cravino, A. From One- to Three-Dimensional Organic Semiconductors: In Search of the Organic Silicon? *Adv. Mater.* **2007**, *19*, 2045–2060.
6. Peet, J.; Heeger, A. J.; Bazan, G. C. "Plastic" Solar Cells: Self-Assembly of Bulk Heterojunction Nanomaterials by Spontaneous Phase Separation. *Acc. Chem. Res.* **2009**, *42*, 1700–1708.
7. Heremans, P.; Cheyns, D.; Rand, B. P. Strategies for Increasing the Efficiency of Heterojunction Organic Solar Cells: Material Selection and Device Architecture. *Acc. Chem. Res.* **2009**, *42*, 1740–1747.
8. Po, R.; Maggini, M.; Camaioni, N. Polymer Solar Cells: Recent Approaches and Achievements. *J. Phys. Chem. C* **2010**, *114*, 695–706.
9. Leclere, P.; Surin, M.; Brocorens, P.; Cavallini, M.; Biscarini, F.; Lazzaroni, R. Supramolecular Assembly of Conjugated Polymers: From Molecular Engineering to Solid-State Properties. *Mater. Sci. Eng. Res.* **2006**, *55*, 1–56.
10. Facchetti, A. π-Conjugated Polymers for Organic Electronics and Photovoltaic Cell Applications. *Chem. Mater.* **2011**, *23*, 733–758.
11. Gearba, R. I.; Mills, T.; Morris, J.; Pindak, R.; Black, C. T.; Zhu, X. Y. Quantifying Interfacial Electric Fields and Local Crystallinity in Polymer-Fullerene Bulk-Heterojunction Solar Cells. *Adv. Funct. Mater.* **2011**, *21*, 2666–2673.
12. Sherwood, G. A.; Cheng, R.; Chacon-Madrid, K.; Smith, T. M.; Peteanu, L. A.; Wildeman, J. Chain Length and Substituent Effects on the Formation of Excimer-like States in Nanoaggregates of CN-PPV Model Oligomers. *J. Phys. Chem. C* **2010**, *114*, 12078–12089.
13. Spano, F. C. The Spectral Signatures of Frenkel Polarons in H- and J-Aggregates. *Acc. Chem. Res.* **2010**, *43*, 429–439.
14. Spano, F. C.; Clark, J.; Silva, C.; Friend, R. H. Determining Exciton Coherence from the Photoluminescence Spectral Line Shape in Poly(3-Hexylthiophene) Thin Films. *J. Chem. Phys.* **2009**, *130*, 074904.
15. Clark, J.; Chang, J. F.; Spano, F. C.; Friend, R. H.; Silva, C. Determining Exciton Bandwidth and Film Microstructure in Polythiophene Films Using Linear Absorption Spectroscopy. *Appl. Phys. Lett.* **2009**, *94*, 163306.
16. Spano, F. C. Modeling Disorder in Polymer Aggregates: The Optical Spectroscopy of Regioregular Poly(3-hexylthiophene) Thin Films. *J. Chem. Phys.* **2005**, *122*, 234701.
17. Gierschner, J.; Huang, Y. S.; Van Averbeke, B.; Cornil, J.; Friend, R. H.; Beljonne, D. Excitonic *versus* Electronic Couplings in Molecular Assemblies: The Importance of Non-nearest Neighbor Interactions. *J. Chem. Phys.* **2009**, *130*, 044105.
18. Mohn, F.; Gross, L.; Moll, N.; Meyer, G. Imaging the Charge Distribution within a Single Molecule. *Nat. Nanotechnol.* **2012**, 10.1038/NNANO.2012.20.
19. Liscio, A.; Palermo, V.; Samori, P. Probing Local Surface Potential of Quasi-one-dimensional Systems: A KPFM Study of P3HT Nanofibers. *Adv. Funct. Mater.* **2008**, *18*, 907–914.
20. Liscio, A.; Palermo, V.; Fenwick, O.; Braun, S.; Mullen, K.; Fahlman, M.; Cacialli, F.; Samori, P. Local Surface Potential of π-Conjugated Nanostructures by Kelvin Probe Force Microscopy: Effect of the Sampling Depth. *Small* **2011**, *7*, 634–639.
21. Palermo, V.; Palma, M.; Samori, P. Electronic Characterization of Organic Thin Films by Kelvin Probe Force Microscopy. *Adv. Mater.* **2006**, *18*, 145–164.
22. Liscio, A.; Palermo, V.; Samori, P. Nanoscale Quantitative Measurement of the Potential of Charged Nanostructures by Electrostatic and Kelvin Probe Force Microscopy: Unraveling Electronic Processes in Complex Materials. *Acc. Chem. Res.* **2010**, *43*, 541–550.
23. Palermo, V.; Liscio, A.; Palma, M.; Surin, M.; Lazzaroni, R.; Samori, P. Exploring Nanoscale Electrical and Electronic Properties of Organic and Polymeric Functional Materials by Atomic Force Microscopy Based Approaches. *Chem. Commun.* **2007**, 3326–3337.
24. Melitz, W.; Shen, J.; Kummel, A. C.; Lee, S. Kelvin Probe Force Microscopy and Its Application. *Surf. Sci. Rep.* **2011**, *66*, 1–27.
25. Groves, C.; Reid, O. G.; Ginger, D. S. Heterogeneity in Polymer Solar Cells: Local Morphology and Performance in Organic Photovoltaics Studied with Scanning Probe Microscopy. *Acc. Chem. Res.* **2010**, *43*, 612–620.
26. Barth, C.; Foster, A. S.; Henry, C. R.; Shluger, A. L. Recent Trends in Surface Characterization and Chemistry with High-Resolution Scanning Force Methods. *Adv. Mater.* **2011**, *23*, 477–501.
27. Puntambekar, K.; Dong, J. P.; Haugstad, G.; Frisbie, C. D. Structural and Electrostatic Complexity at a Pentacene/Insulator Interface. *Adv. Funct. Mater.* **2006**, *16*, 879–884.
28. Taylor, D. M.; Bayes, G. F. Calculating the Surface-Potential of Unionized Monolayers. *Phys. Rev. E* **1994**, *49*, 1439–1449.

29. Maldonado, S.; Smith, T. J.; Williams, R. D.; Morin, S.; Barton, E.; Stevenson, K. J. Surface Modification of Indium Tin Oxide *via* Electrochemical Reduction of Aryldiazonium Cations. *Langmuir* **2006**, *22*, 2884–2891.
30. Zuppiroli, L.; Si-Ahmed, L.; Kamaras, K.; Nuesch, F.; Bussac, M. N.; Ades, D.; Siove, A.; Moons, E.; Gratzel, M. Self-Assembled Monolayers as Interfaces for Organic Opto-electronic Devices. *Eur. Phys. J. B* **1999**, *11*, 505–512.
31. Sugimura, H.; Hayashi, K.; Saito, N.; Nakagiri, N.; Takai, O. Surface Potential Microscopy for Organized Molecular Systems. *Appl. Surf. Sci.* **2002**, *188*, 403–410.
32. Fujihira, M. Kelvin Probe Force Microscopy of Molecular Surfaces. *Annu. Rev. Mater. Sci.* **1999**, *29*, 353–380.
33. Aruta, C.; D'Angelo, P.; Barra, M.; Ausanio, G.; Cassinese, A. Improved Structural Ordering in Sexithiophene Thick Films Grown on Single Crystal Oxide Substrates. *Appl. Phys. A: Mater. Sci. Process* **2009**, *97*, 387–394.
34. Kaake, L. G.; Barbara, P. F.; Zhu, X. Y. Intrinsic Charge Trapping in Organic and Polymeric Semiconductors: A Physical Chemistry Perspective. *J. Phys. Chem. Lett.* **2010**, *1*, 628–635.